Supporting Information:

Leveraging Cu_2SnTe_3 Additives for Improved Thermoelectric Figure of Merit and Module Efficiency in $Bi_{0.5}Sb_{1.5}Te_3$-Based Composites

Qiaoyan Pan,† Kaikai Pang,† Qiang Zhang,* Yan Liu, Huilie Shi, Jingsong Li, Wenjie Zhou, Qianqian Sun, Yuyou Zhang, Xiaojian Tan, Peng Sun, Jiehua Wu,* Guo-Qiang Liu, Jun Jiang*

Q. Pan, K. Pang, Dr. Q. Zhang, W. Zhou, Q. Sun, Y. Zhang, Prof. X. Tan, P. Sun, J. Wu, Prof. G.-Q. Liu, Prof. J. Jiang

Ningbo Institute of Materials Technology and Engineering, Chinese Academy of Sciences

Ningbo 315201, China

E-mail: qiangzhang@nimte.ac.cn, jiehuawu@nimte.ac.cn, jjun@nimte.ac.cn

Q. Pan, Dr. Q. Zhang, Q. Sun, Prof. X. Tan, P. Sun, J. Wu, Prof. G.-Q. Liu, Prof. J. Jiang

University of Chinese Academy of Sciences

Beijing 100049, China

Y. Liu, H. Shi, J. Li

Research Institute of Nuclear Power Operation

Wuhan 430223, China

† These authors contribute equally.

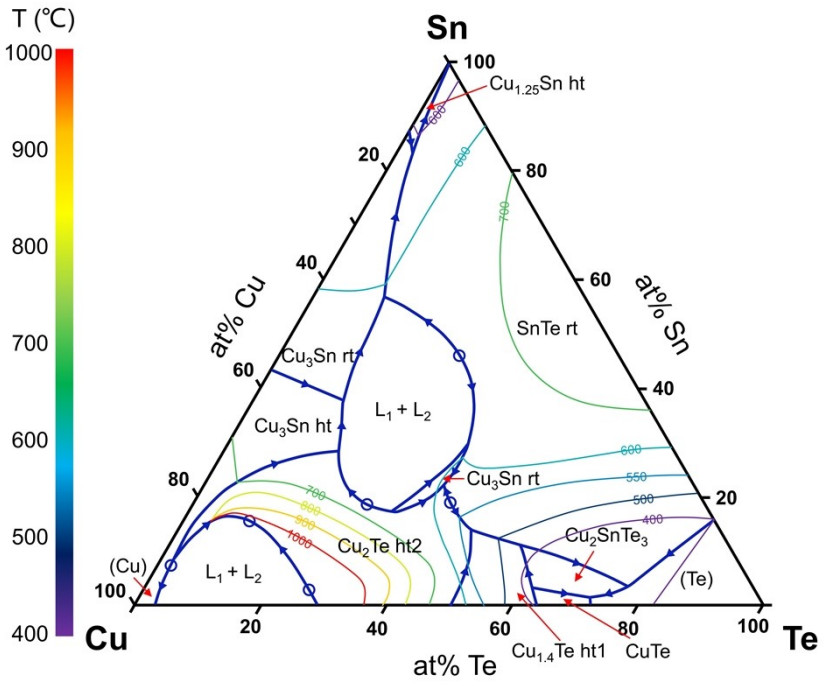

Figure S1. The liquidus projection of the ternary phase diagram for the Cu-Sn-Te system.[1]

Table S1. The XRD refinement results for lattice parameters of $Bi_{0.5}Sb_{1.5}Te_3$ and $Bi_{0.5}Sb_{1.5}Te_3$ + 0.08 wt % Cu_2SnTe_3 representative samples.

Samples		$x = 0$	$x = 0.08$
Lattice parameters (Å)	a/b	4.2967	4.2949
	c	30.4862	30.4914

At the molten temperature of $Bi_{0.5}Sb_{1.5}Te_3$, Cu_2SnTe_3 exhibits instability and undergoes facile decomposition, which may cause Cu (1.17 Å) or Sn (1.40 Å) to replace Sb (1.41 Å) or Bi (1.46 Å), thereby slightly reducing the *a*- and *b*-axis. On the contrary, the *c*-axis slightly increases, possibly due to part of Cu atoms entering the van der Waals interlayer positions. The variation of lattice constants indicates that Cu_2SnTe_3 has been successfully doped into $Bi_{0.5}Sb_{1.5}Te_3$ and formed a stable solid solution. In this work, the variations in the lattice parameters of the samples are inconsequential, given the trace amount of Cu_2SnTe_3.

The calculation of orientation factor *F*

The orientation factor (*F*), serving as an indicator of the orientation degree in layered-structural samples, is calculated using the Lotgering method and expressed by the following equation:[2]

$$F = \frac{P - P_0}{1 - P_0}$$

$$P = \frac{\sum I(00l)}{\sum I(hkl)}$$

$$P_0 = \frac{\sum I_0(00l)}{\sum I_0(hkl)}$$

where Σ*I*(*00l*) represents the total intensity of all (*00l*) planes diffraction peaks, Σ*I*(*hkl*) represents the total intensity of all (*hkl*) diffraction peaks, and *P* is the ratio of (*00l*) plane intensity to total intensity in the measured data. Similarly, ΣI_0(*00l*), ΣI_0(*hkl*), and P_0 represent the corresponding parts of the standard powder diffraction file. In the X-ray patterns of incompletely oriented materials, the (*hkl*) reflections still occur, and the ratio of the intensity of the (*00l*) and (*hkl*) reflections increases with stronger orientation. The orientation factor *F* takes values ranging from 0 to 1, indicating from no preferred orientation to complete orientation.

For a series of samples, the calculated orientation factors F_{00l} are summarized in the following table. It can be seen that the F_{00l} values of the samples prepared by ball milling and spark plasma sintering methods are very small, ranging from 0.045 to 0.070.

Table S2. Orientation factors F_{00l} for the $Bi_{0.5}Sb_{1.5}Te_3$ + x wt% Cu_2SnTe_3 samples at room temperature.

x	F_{00l}
0	0.05641
0.04	0.06967
0.06	0.06674
0.08	0.05499
0.10	0.04691

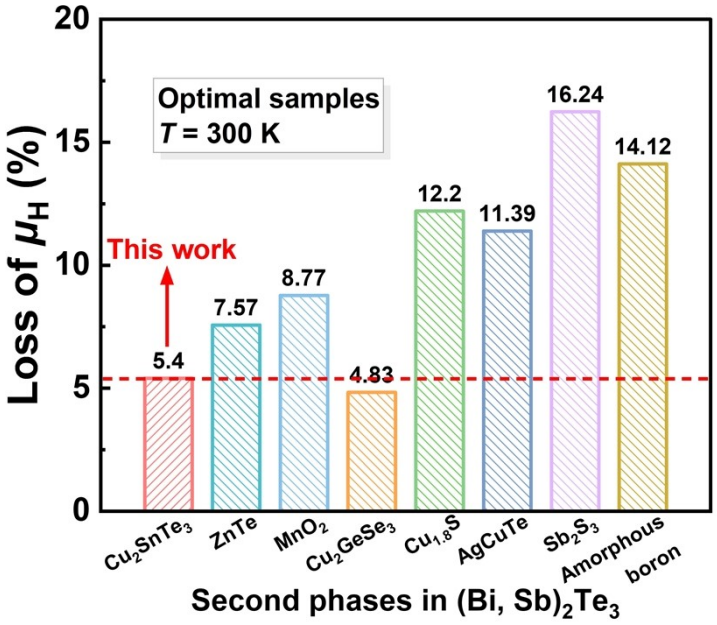

Figure S2. Comparison of the mobility loss of optimal samples at 300 K due to the second phases with different types and concentrations.

Single Parabolic Band (SPB) model

The SPB model, derived from the Boltzmann transport equation, assumes that only one parabolic band contributes to the electron conduction and that acoustic phonon scattering dominates.[3] With the SPB model, the bidirectional analysis of electrical transport theory and experimental data can be realized. The main equations are as follows:[4]

Fermi integral,

$$F_j(\eta) = \int_0^\infty \frac{\xi^j}{1 + e^{\xi - \eta}} d\xi$$

The Seebeck coefficient,

$$S(\eta) = \frac{k_B}{e}\left[\frac{(r + 5/2)F_{(r + 3/2)}(\eta)}{(r + 3/2)F_{(r + 1/2)}(\eta)} - \eta\right]$$

The Hall carrier concentration,

$$n_H = \frac{1}{eR_H} = \frac{8\pi(2m_d^* k_B T)^{3/2}(r + 3/2)^2 F_{(r + 1/2)}{}^2(\eta)}{3h^3 \qquad (2r + 3/2)F_{(2r + 1/2)}(\eta)}$$

The Hall mobility,

$$\mu_H = \left[\frac{e\pi h^4 \qquad C_l}{\sqrt{2}(k_B T)^{3/2} E_{def}{}^2 (m_d^*)^{5/2}}\right]\frac{(2r + 3/2)F_{(2r + 1/2)}(\eta)}{(r + 3/2)^2 F_{(r + 1/2)}(\eta)}$$

Lorenz Factor,

$$L = (\frac{k_B}{e})^2\left\{\frac{(r + 7/2)F_{(r + 5/2)}(\eta)}{(r + 3/2)F_{(r + 3/2)}(\eta)} - \left[\frac{(r + 5/2)F_{(r + 3/2)}(\eta)}{(r + 3/2)F_{(r + 1/2)}(\eta)}\right]^2\right\}$$

In the above equations, m_d^* is the density-of-states effective mass, C_l is the elastic constant for longitudinal vibrations, E_{def} is the deformation potential coefficient characterizing the strength of carriers scattered by acoustic phonons, and η is the reduced Fermi level. When charge carriers are scattered by acoustic phonons, $r = -1/2$.

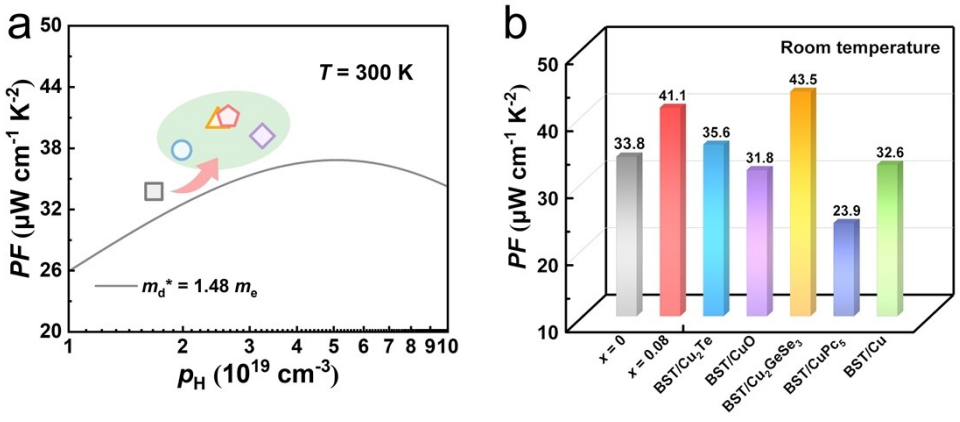

Figure S3. (a) Carrier concentration dependence of power factor for a series of samples at 300 K. (b) Comparison of power factors at room temperature of $x = 0$ and $x = 0.08$ samples with previously reported (Bi, Sb)$_2$Te$_3$-based materials.[5–9]

Calculation of κ_{ph} and κ_{bip}

Disregarding the bipolar effect at lower temperatures, the value of $\kappa_{ph} + \kappa_{bip}$ is approximately equal to the value of κ_{ph}. The κ_{ph} data around 300 K can be fitted with the expression $\kappa_{ph} = aT^{-1} + b$, where a and b are the fitting parameters. Then the fitted κ_{ph} is obtained by extrapolating the equation to 500 K. Finally, the fitted κ_{ph} and calculated κ_e are subtracted from the measured κ_{tot} to obtain the κ_{bip} values for all samples between 300~500 K.

Table S3. Fitting parameters for all samples using the expression of $\kappa_{ph} = aT^{-1} + b$.

	$Bi_{0.5}Sb_{1.5}Te_3 + x$ wt% Cu_2SnTe_3				
	$x = 0$	$x = 0.04$	$x = 0.06$	$x = 0.08$	$x = 0.10$
a	10.25821	6.26283	7.22138	12.37915	13.85580
b	0.60148	0.55284	0.51630	0.46933	0.44540

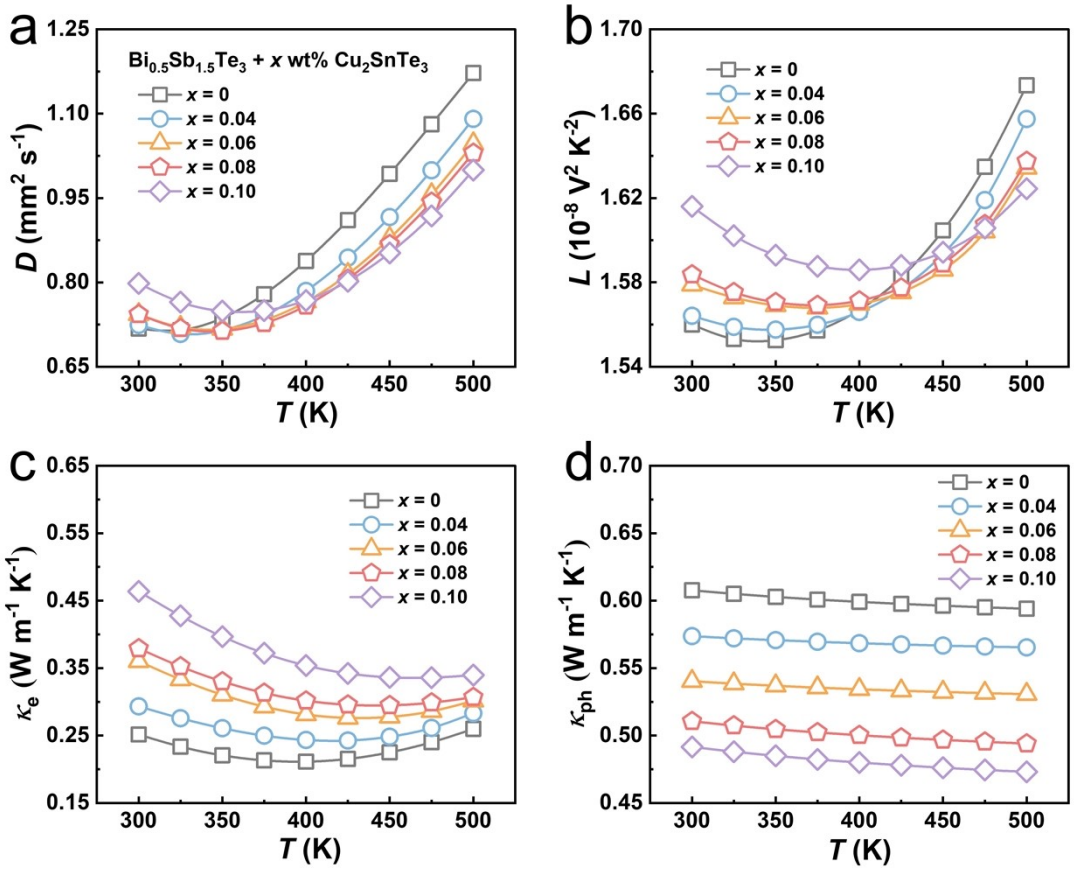

Figure S4. Temperature dependence of (a) thermal diffusivity D, (b) Lorentz factor L, (c) electronic thermal conductivity κ_e, and (d) lattice thermal conductivity κ_{ph} of $Bi_{0.5}Sb_{1.5}Te_3$ + x wt% Cu_2SnTe_3 series samples.

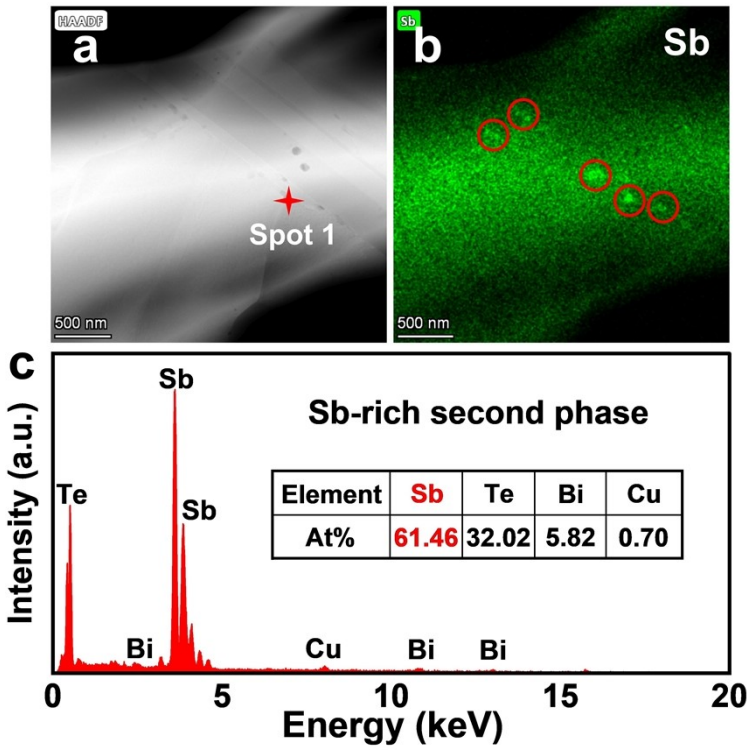

Figure S5. (a) HAADF image and (b) the corresponding EDS elemental mapping of Sb-enriched area. (c) Actual atomic fraction of "Spot 1" in (a).

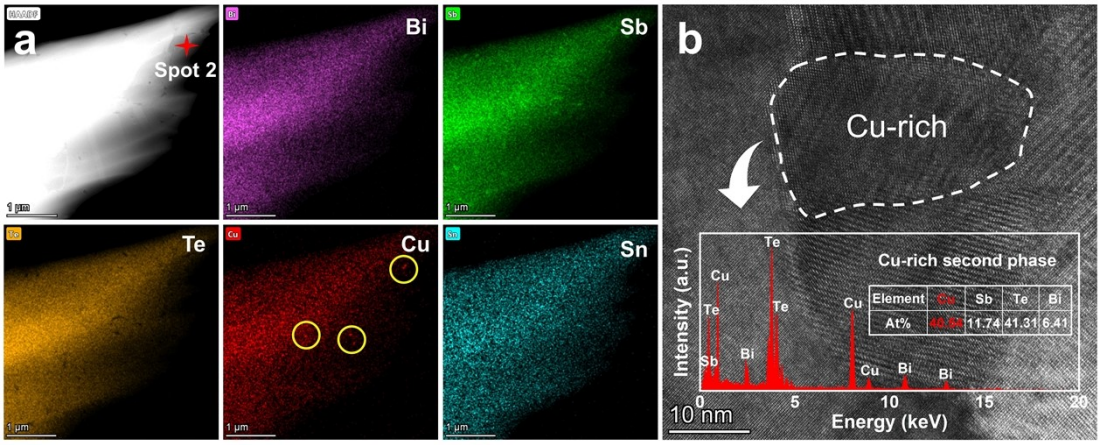

Figure S6. (a) HAADF image and the corresponding EDS elemental mappings of Cu-enriched area. (b) High-resolution TEM image and corresponding actual atomic fraction of "Spot 2" in (a) indicate the existence of Cu-enriched area.

Debye-Callaway model

The Debye-Callaway model, which visualizes the contribution of multi-scale defects to phonon scattering, can explain the mechanism for the reduced lattice thermal conductivity of $Bi_{0.5}Sb_{1.5}Te_3$ + x wt% Cu_2SnTe_3 samples. Here the equation for κ_{ph} is as follows:

$$\kappa_{ph} = \frac{k_B}{2\pi^2 v}\left(\frac{k_B T}{\hbar}\right)^3 \int_0^{\Theta_D/T} \tau_{tot}(x) \frac{x^4 e^x}{(e^x - 1)^2} dx$$

The integral term along with the coefficients in the equation is the spectral lattice thermal conductivity κ_s, namely:

$$\kappa_s = \frac{k_B}{2\pi^2 v}\left(\frac{k_B T}{\hbar}\right)^3 \frac{x^4 e^x}{\tau_{tot}^{-1}(x)(e^x - 1)^2}$$

where $x = \hbar\omega/k_B T$ is the reduced phonon frequency, $\hbar$ is the reduced Plank constant, ω is the phonon frequency, k_B is the Boltzmann constant, T is the absolute temperature, v is the in-plane average velocity of phonon, θ_D is the Debye temperature. τ_{tot} is the frequency-dependent total relaxation time, which can be obtained according to Matthiessen's rule:

$$\tau_{tot}^{-1} = \tau_U^{-1} + \tau_{PD}^{-1} + \tau_{GB}^{-1} + \tau_D^{-1} + \tau_{SP}^{-1}$$

For thermoelectric materials, phonon scattering sources with different specific frequencies mainly include Umklapp scattering (U), point defects scattering (PD), grain boundaries scattering (GB), dislocations scattering (D), and second phases scattering (SP).

The relaxation time associated with Umklapp phonon-phonon scattering (τ_U) can be calculated by the following equation:

$$\tau_U^{-1} = A_N \frac{2}{(6\pi^2)^{1/3}} \frac{k_B V^{1/3} \gamma^2 \omega^2 T}{M v^3}$$

where V, γ, and M represent atomic volume, Gruneisen parameter, and atomic mass, respectively. A_{N} can be determined by fitting experimental data of crystalline materials in the literature.

The relaxation time associated with point defects scattering (τ_{PD}) is calculated from:

$$\tau_{PD}^{-1} = \frac{V\omega^4}{4\pi v^3}\Gamma$$

where Γ is the point defects scattering parameter expressed as:

$$\Gamma = x(1-x)\left[\left(\frac{\Delta M}{M}\right)^2 + \frac{2}{9}\left\{(G+6.4\gamma)\frac{1+r}{1-r}\right\}^2\left(\frac{\Delta a}{a}\right)^2\right]$$

where x, G, r, ΔM and Δa are the fractional concentration of either of constituents, the parameter representing the ratio of fractional change of bulk modulus to that of local bond length, Poisson's ratio, the difference in mass, and the difference in lattice constants, respectively.

The relaxation time associated with grain boundaries scattering (τ_{GB}) is related to the average grain size d, the relevant formula is as follows:

$$\tau_{GB}^{-1} = \frac{v}{d}$$

The relaxation time associated with dislocations scattering (τ_D) includes dislocation core scattering relaxation time (τ_{DC}) and dislocation strain scattering relaxation time. The formulas are as follows:

$$\tau_{DC}^{-1} = N_D\frac{V^{\frac{4}{3}}}{v^2}\omega^3$$

$$\tau_{DS}^{-1} = 0.6B_D^2N_D(\gamma+\Delta\gamma)^2\omega\left\{\frac{1}{2} + \frac{1}{24}\left(\frac{1-2r}{1-r}\right)^2\left[1+\sqrt{2}\left(\frac{v_L}{v_T}\right)\right]^2\right\}$$

$$\Delta\gamma = \frac{V_{ST}C_0K}{k_BT_a}(\gamma\alpha^2 - \alpha\beta)$$

$$\alpha = \frac{V_{BT}-V_{ST}}{V_{ST}}$$

$$\beta = \frac{M_{ST} - M_{BT}}{2M_{ST}}$$

where N_D, B_D, $\Delta\gamma$, υ_L, υ_T, C_0, K, T_a are dislocation density, effective Burger's vector, change in Grüneisen parameter, longitudinal phonon velocity, transverse phonon velocity, concentration of Bi_2Te_3 in $Bi_{0.5}Sb_{1.5}Te_3$, bulk modulus of Sb_2Te_3, and sample sintering temperature, respectively. In the above equation, BT and ST are abbreviations for Bi_2Te_3 and Sb_2Te_3.

The relaxation time associated with second phases scattering (τ_{SP}) is calculated from:

$$\tau_{SP}^{-1} = v\left[\left(2\pi R^2\right)^{-1} + \left(\frac{4}{9}\pi R^2(\Delta D/D)^2(\omega R/v)^4\right)^{-1}\right]^{-1} N_P$$

where D, ΔD, R, and Np are the mass density of the matrix, the density difference between the matrix and the nanoscale second phase precipitates, the average radius of the second phases, and the number density of the second phases.

Table S4. Specific parameters for calculating the lattice thermal conductivity of the $Bi_{0.5}Sb_{1.5}Te_3$ + 0.08 wt% Cu_2SnTe_3 sample in the Debye-Callaway model.

Parameters	Description	Values	Methods
θ_D	Debye temperature	94 K	[10]
d	Grain size	2×10^{-6} m	Exp.
A_N	Prefactor of Umklapp scattering relaxation time	2.6	[11]
M_{BT}	Atomic mass of Bi_2Te_3	2.79×10^{-25} kg	-
M_{ST}	Atomic mass of Sb_2Te_3	2.07×10^{-25} kg	-
V_{BT}	Atomic volume of Bi_2Te_3	3.40×10^{-29} m^3	-
V_{ST}	Atomic volume of Sb_2Te_3	3.31×10^{-29} m^3	-

V	Average atomic volume of $Bi_{0.5}Sb_{1.5}Te_3$	31.26 Å^3	[12]
N_d	Dislocation density	4.17×10^{10} cm^{-2}	Exp.
B_D	Effective Burger's vector	1.2×10^{-9} m	Fitted
γ	Grüneisen parameter	2.33	[13]
v	In-plane average velocity of phonon	2147 m s^{-1}	[13]
v_L	Longitudinal phonon velocity	2884 m s^{-1}	[14]
v_T	Transverse phonon velocity	1780 m s^{-1}	[13]
r	Poisson's ratio	0.24	[12]
N_P	Number density of second phases	7.33×10^{21} m^{-3}	Exp.
R	Average radius of second phases	20 nm	Exp.
D	Density of matrix	6.65 g cm^{-3}	Exp.
C_0	Concentration of Bi_2Te_3 in $Bi_{0.5}Sb_{1.5}Te_3$	0.25	-
K	Bulk modulus	44.8 GPa	[13]
T_a	Sample Sintering temperature	693 K	Exp.

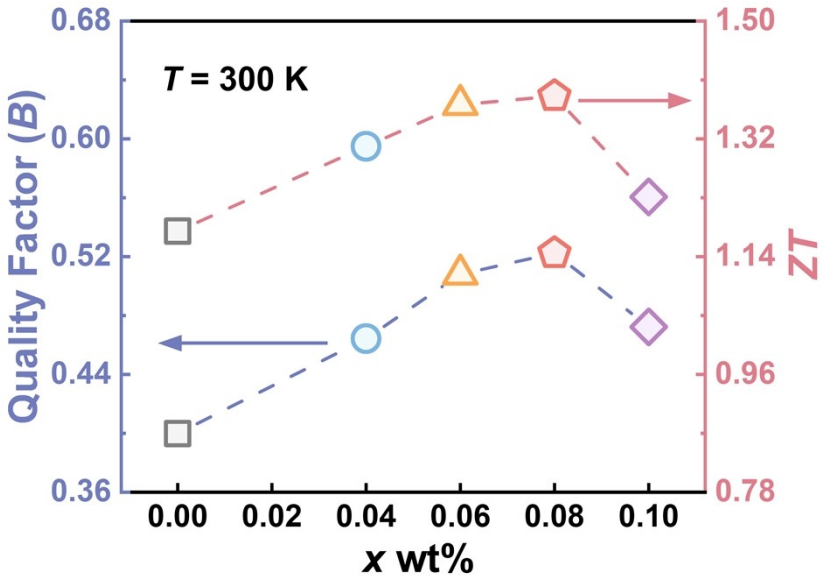

Figure S7. Variation of thermoelectric quality factor (*B*) and figure of merit *ZT* with Cu_2SnTe_3 content at 300 K. The similar variation trend of the two curves indicates that higher *B* is obtained by doping appropriate amount of Cu_2SnTe_3, thus increasing *ZT* value.

The calculation of average *ZT* and engineering *ZT*

The average *ZT* (ZT_{ave}) is an important parameter for evaluating the thermoelectric properties of materials within a certain temperature range, which can be calculated by the following formula:[15]

$$ZT_{ave} = \frac{1}{T_h - T_c}\int_{T_c}^{T_h} ZT(T)\, dT$$

where T_h and T_c are the temperatures of the hot side and the cold side, respectively.

The engineering *ZT* (ZT_{eng}) provides a practical method for evaluating the maximum thermoelectric conversion efficiency (η_{max}). The calculation formula of ZT_{eng} is as follows:[16]

$$(ZT)_{eng} = Z_{eng}\Delta T = \frac{\left(\int_{T_c}^{T_h} S(T)dT\right)^2}{\int_{T_c}^{T_h} \rho(T)dT \int_{T_c}^{T_h} \kappa(T)dT}\Delta T = \frac{(PF)_{eng}}{\int_{T_c}^{T_h} \kappa(T)dT}\Delta T$$

where $S(T)$, $\rho(T)$, $\kappa(T)$ are Seebeck coefficient, electrical resistivity and total thermal conductivity, all of which are temperature dependent.

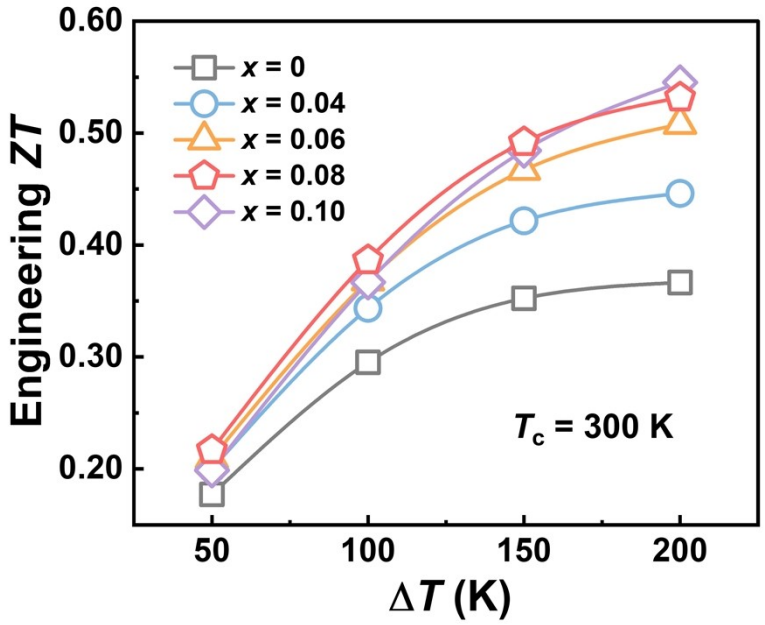

Figure S8. Calculated engineering *ZT* at the cold-side temperature (T_c) of 300 K.

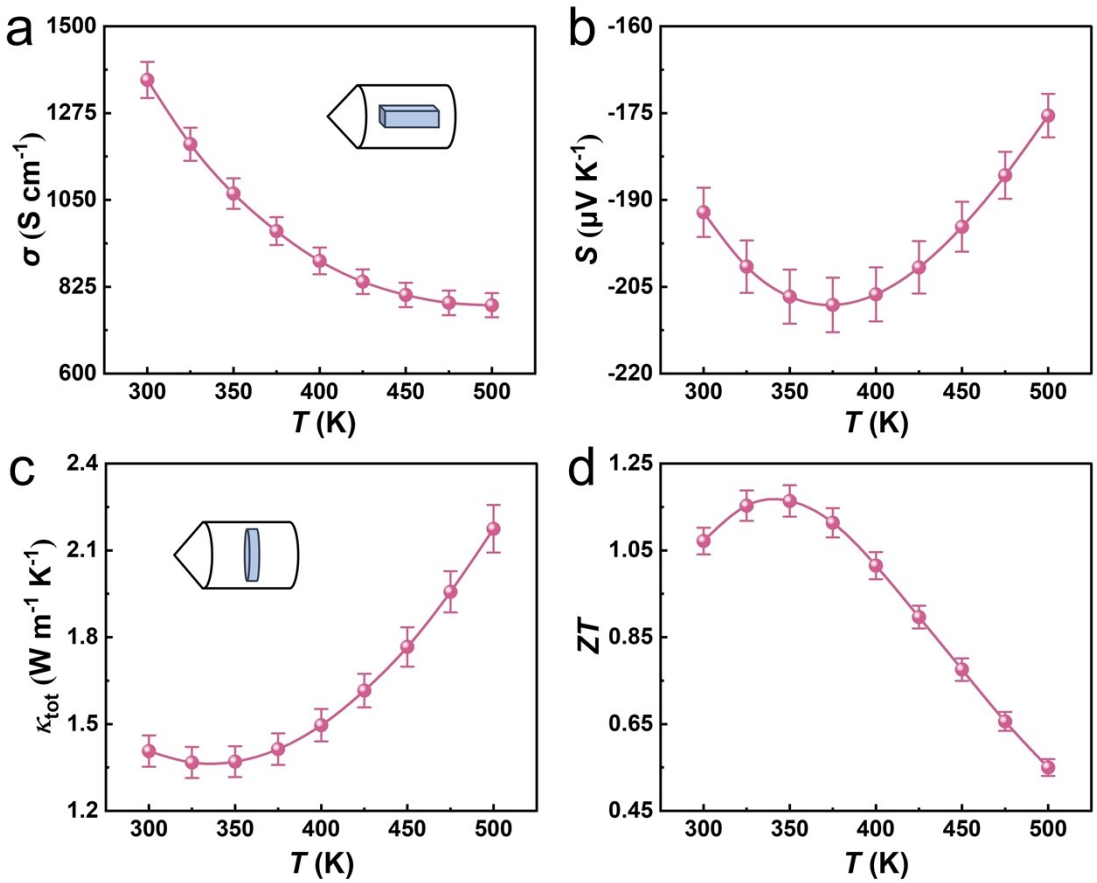

Figure S9. Temperature dependence of (a) electrical conductivity, (b) Seebeck coefficient, (c) total thermal conductivity, and (d) *ZT* value for previously reported zone-melted $Bi_2Te_{2.7}Se_{0.3}$ materials used to assemble the thermoelectric module. The orientation of the test samples in the ingot is shown in figures (a) and (c).

Multi-physics field simulations

Multi-physics simulations were performed using the COMSOL program and its dedicated "thermoelectric effect" module to analyze the output performance. Seventeen sets of thermoelectric module, comprising TE legs, Cu electrodes, insulating ceramic substrates, and loads, were modeled in three dimensions. The temperature-dependent parameters (S, σ, and κ_{tot}) for both our *p*-type $Bi_{0.5}Sb_{1.5}Te_3$ + 0.08 wt% Cu_2SnTe_3 and zone-melted *n*-type counterparts were integrated as input. Theoretical conversion efficiency (depicted in Figure 6b) and output power (illustrated in Figure S10) were simulated by adjusting the cross-sectional area ratio of *p*- and *n*-type legs, along with the ratio of leg height to total section area.

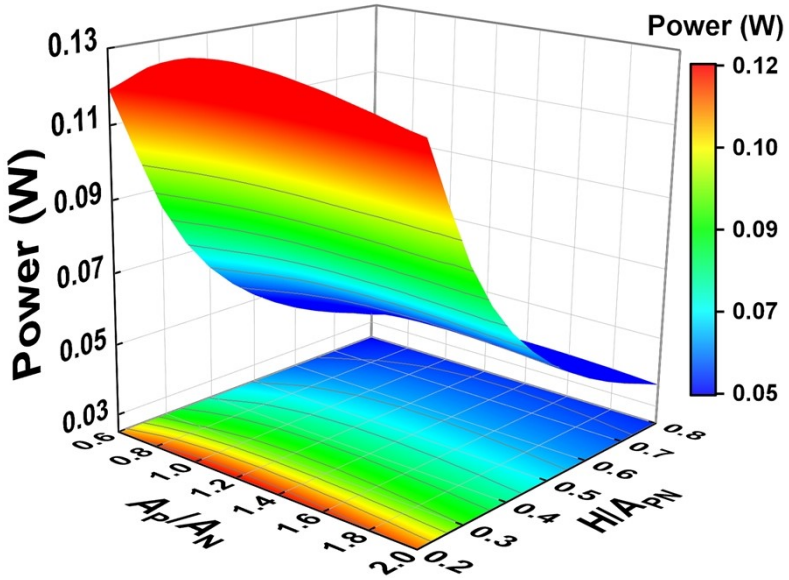

Figure S10. Multi-physics field simulated output power as a function of the cross-sectional area ratio of *p*- and *n*-type legs and the ratio of leg height versus total section area.

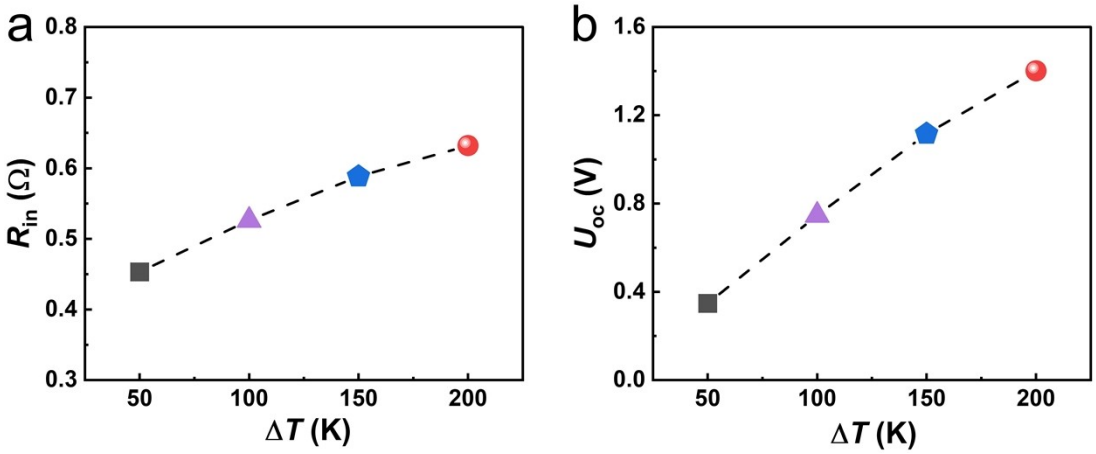

Figure S11. (a) Internal resistance R_{in} and (b) open-circuit voltage U_{oc} change with temperature difference ΔT.

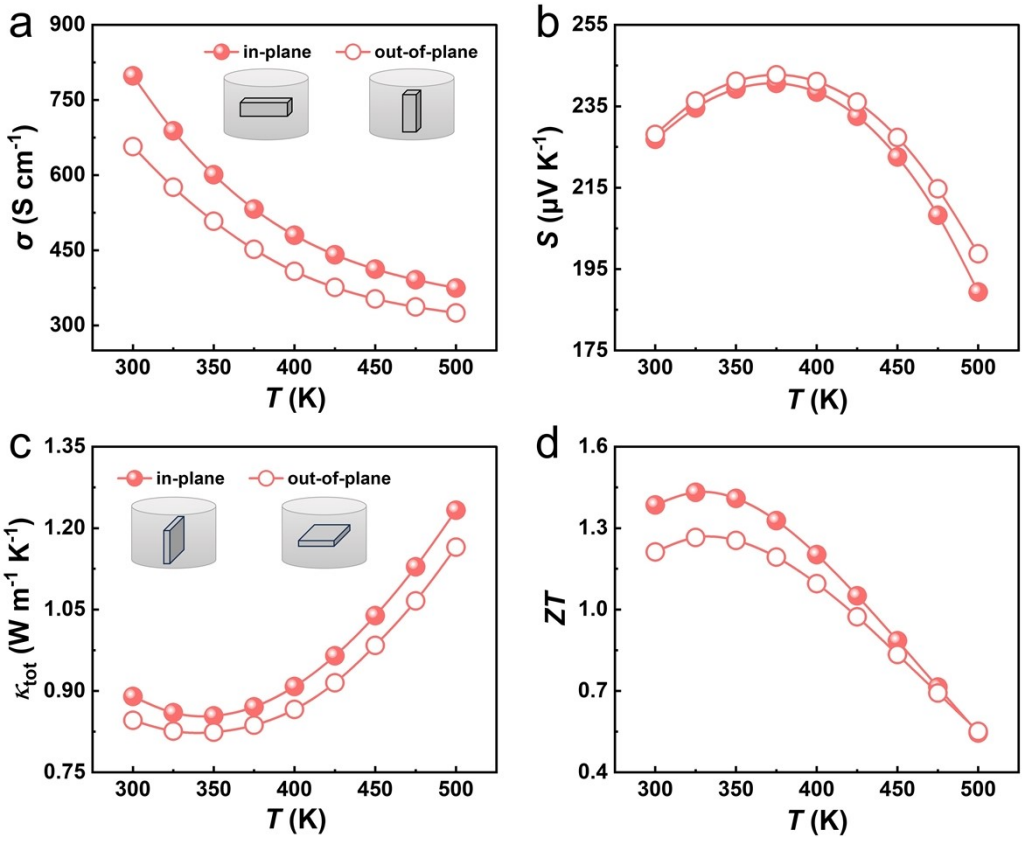

Figure S12. Comparison of electronic and thermal transport properties of the representative $Bi_{0.5}Sb_{1.5}Te_3$ + 0.08 wt% Cu_2SnTe_3 sample along both the in-plane and out-of-plane directions, including (a) electrical conductivity, (b) Seebeck coefficient, (c) total thermal conductivity, and (d) *ZT* value.

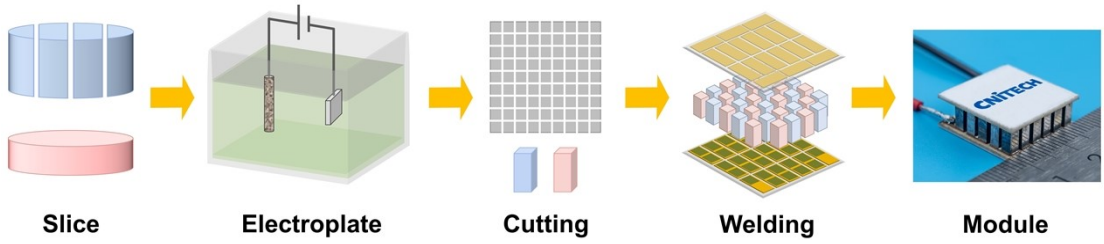

Figure S13. Schematic diagram of the process for manufacturing materials into a TE module.

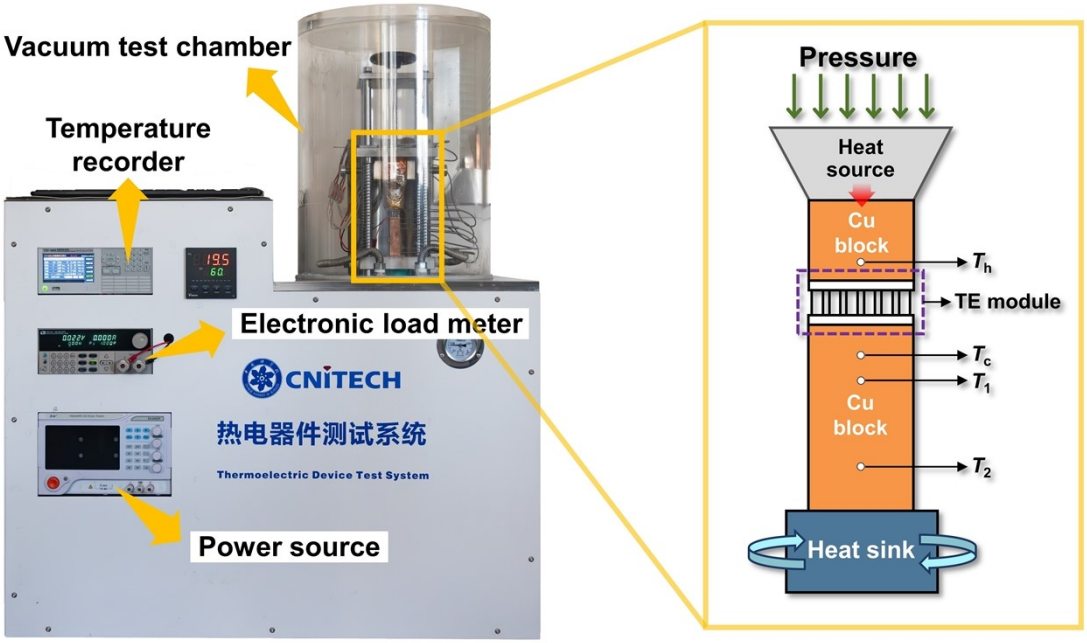

Figure S14. The test system for measuring the conversion efficiency and output power of thermoelectric modules.

Synthesis of Cu_2SnTe_3 compound

High-purity Cu (copper wires, 99.99 %), Sn (granules, 99.999 %) and Te (chunks, 99.999 %) were weighed and mixed according to the stoichiometric ratio of Cu_2SnTe_3. Then the vacuum-sealed quartz tube containing the feedstock elements was placed in the pit furnace heated at 1273 K for 300 min, continued heating at 923 K for 300 min, and slowly cooled to room temperature. Subsequently, the obtained ingot was ball milled for 30 min using a high-speed vibrating ball mill (MSK-SFM-3, China) under the protection of argon gas. Finally, the Cu_2SnTe_3 compound powder was sieved through a 300-mesh screen (approximately 50 μm) and stored in argon atmosphere.

References

[1] M. Venkatraman, A. Schlieper, R. Blachnik and B. Gather, *Int. J. Mater. Res.*, 1994, **85**, 354–359.

[2] F. K. Lotgering, *J. Inorg. Nucl. Chem.*, 1959, **9,** 113–123.

[3] J. Zhu, X. Zhang, M. Guo, J. Li, J. Hu, S. Cai, W. Cai, Y. Zhang and J. Sui, *Npj Comput. Mater.*, 2021, **7**, 116.

[4] J. Shen, Z. Chen, S. Lin, L. Zheng, W. Li and Y. Pei, *J. Mater. Chem. C*, 2016, **4**, 209–214.

[5] Q. Shi, X. Zhao, Y. Chen, L. Lin, D. Ren, B. Liu, C. Zhou and R. Ang, *ACS Appl. Mater. Interfaces*, 2022, **14**, 45582–45589.

[6] G. Wu, Z. Yan, X. Wang, X. Tan, K. Song, L. Chen, Z. Guo, G.-Q. Liu, Q. Zhang, H. Hu and Jun Jiang, *ACS Appl. Mater. Interfaces*, 2021, **13**, 57514−57520.

[7] K. Pang, M. Yuan, Q. Zhang, Y. Li, Y. Zhang, W. Zhou, G. Wu, X. Tan, J. G. Noudem, C. Cui, H. Hu, J. Wu, P. Sun, G.-Q. Liu and J. Jiang, *Small*, 2023, 2306701.

[8] X. Wang, J. Cheng, L. Yin, Z. Zhang, X. Wang, J. Sui, X. Liu, J. Mao, F. Cao and Q. Zhang, *Adv. Funct. Mater.*, 2022, **32**, 2200307.

[9] F. Hao, P. Qiu, Y. Tang, S. Bai, T. Xing, H.-S. Chu, Q. Zhang, P. Lu, T. Zhang, D. Ren, J. Chen, X. Shi and L. Chen, *Energy Environ. Sci.*, 2016, **9**, 3120–3127.

[10] D. Bessas, I. Sergueev, H.-C. Wille, J. Perßon, D. Ebling and R. P. Hermann, *Phys. Rev. B*, 2012, **86**, 224301.

[11] Y. Yu, D.-S. He, S. Zhang, O. Cojocaru-Mirédin, T. Schwarz, A. Stoffers, X.-Y. Wang, S. Zheng, B. Zhu, C. Scheu, D. Wu, J.-Q. He, M. Wuttig, Z.-Y. Huang and F.-Q. Zu, *Nano Energy*, 2017, **37**, 203–213.

[12] E. S. Toberer, A. Zevalkink and G. J. Snyder, *J. Mater. Chem.*, 2011, **21**, 15843.

[13] X. Chen, H. D. Zhou, A. Kiswandhi, I. Miotkowski, Y. P. Chen, P. A. Sharma, A. L. Lima Sharma, M. A. Hekmaty, D. Smirnov and Z. Jiang, *Appl. Phys. Lett.*, 2011, **99**, 261912.

[14] F. Yang, T. Ikeda, G. J. Snyder and C. Dames, *J. Appl. Phys.*, 2010, **108**, 034310.

[15] X. Zhang and L.-D. Zhao, *J. Materiomics*, 2015, **1**, 92–105.

[16] H. S. Kim, W. Liu, G. Chen, C.-W. Chu and Z. Ren, *Proc. Natl. Acad. Sci. U.S.A.*, 2015, **112**, 8205–8210.